# Location Uncertainty Principle: Toward the Definition of Parameter-free Motion Estimators *

Shengze Cai, Etienne Mémin, Pierre Dérian, Chao Xu

▶ **To cite this version:**

Shengze Cai, Etienne Mémin, Pierre Dérian, Chao Xu. Location Uncertainty Principle: Toward the Definition of Parameter-free Motion Estimators *. EMMCVPR 2017 - 11th International Conference on Energy Minimization Methods in Computer Vision and Pattern Recognition, Oct 2017, Venice, Italy. pp.1-15. hal-01654184

**HAL Id: hal-01654184**
**https://inria.hal.science/hal-01654184**

Submitted on 3 Dec 2017

**HAL** is a multi-disciplinary open access archive for the deposit and dissemination of scientific research documents, whether they are published or not. The documents may come from teaching and research institutions in France or abroad, or from public or private research centers.

L'archive ouverte pluridisciplinaire **HAL**, est destinée au dépôt et à la diffusion de documents scientifiques de niveau recherche, publiés ou non, émanant des établissements d'enseignement et de recherche français ou étrangers, des laboratoires publics ou privés.

# Location Uncertainty Principle: Toward the Definition of Parameter-free Motion Estimators *

Shengze Cai[1], Etienne Mémin[2], Pierre Dérian[2], and Chao Xu[1]

[1] State Key Laboratory of Industrial Control Technology and the Institute of Cyber-Systems & Control, Zhejiang University, Hangzhou, 310027 Zhejiang, China.
{szcai, cxu}@zju.edu.cn

[2] National Institute for Research in Computer Science and Control (INRIA), Campus Universitaire de Beaulieu, 35042 Rennes, France.
{etienne.memin, pierre.derian}@inria.fr

**Abstract.** In this paper, we propose a novel optical flow approach for estimating two-dimensional velocity fields from an image sequence, which depicts the evolution of a passive scalar transported by a fluid flow. The Eulerian fluid flow velocity field is decomposed into two components: a large-scale motion field and a small-scale uncertainty component. We define the small-scale component as a random field. Then the data term of the optical flow formulation is based on a stochastic transport equation, derived from a location uncertainty principle [17]. In addition, a specific regularization term built from the assumption of constant kinetic energy involves the same diffusion tensor as the one appearing in the data transport term. This enables us to devise an optical flow method dedicated to fluid flows in which the regularization parameter has a clear physical interpretation and can be easily estimated. Experimental evaluations are presented on both synthetic and real images. Results indicate very good performance of the proposed parameter-free formulation for turbulent flow motion estimation.

## 1 Introduction

Motion estimation techniques are becoming increasingly important in the study of fluid dynamics. Extracting the velocity fields from image sequences allows the researchers to get a deeper insight into the complex and unsteady fluid flows. First proposed by Horn and Schunck [13], optical flow has been intensively studied in the computer vision community, and a huge number of variations have been presented in the literature, such as [2], [3], [18], [21]. All these methods rely on the fundamental assumption of a brightness conservation along a point trajectory:

$$\frac{\mathrm{d}f}{\mathrm{d}t} = \frac{\partial f}{\partial t} + \nabla f \cdot \boldsymbol{\omega} = 0. \tag{1}$$

In this transport equation, referred to as the optical flow constraint (OFC), $\nabla$ denotes the gradient operator, $f$ and $\boldsymbol{\omega}$ the intensity of the image and the motion field, respectively.

* This work was supported by the National Natural Science Foundation of China under Grant 61473253, and the Foundation for Innovative Research Groups of the National Natural Science Foundation of China under Grant 61621002.

For variational optical flow approaches, the OFC equation is associated with a spatial coherency assumption [13], in order to cope with the so called aperture problem. A weighting coefficient balances these two terms in the optic-flow energy functional.

Compared to the correlation-based motion estimators, optical flow methods enable to estimate dense velocity fields and thus potentially lead to motion fields with finer details. In addition, the OFC equation (1) can be combined with various physical constraints to describe the transportation of a fluidic scalar by a motion field. Note that the classical optical flow methods are in general used for estimating rigid motions and rely on a strong smoothing constraint. This constraint is difficult to interpret physically and the weighting coefficient is hard to choose optimally.

The original Horn and Schunck (HS) formulation has been extended in various ways to cope with motion estimation from fluid images. For instance, Corpetti *et al.* [7] presented a fluid-flow dedicated formulation based on the integrated continuity equation (ICE) and a second-order *div-curl* regularizer, that allow preserving better the divergence and the vorticity of the flow. Liu and Shen [16] discussed the relation between optical flow and fluid flow, and suggested to use the projected motion equation. Among the recently-developed techniques, optical flow is also formulated in the forms of orthogonal decomposition [22], wavelet expansion with a higher-order regularization term [10], [15], optimal control scheme [19] or Bayesian stochastic filtering approach [9]. A review on different fluid motion estimation techniques is presented in [12].

Despite a great deal of effort, turbulence modeling and measurement is still a challenging issue in fluid mechanics. Realistic turbulent flows contain small-scale structures that are significant for energy and mass transport. However, the sub-grid scales are not taken into account in the optical flow formulations. To overcome this problem, [5] replaced the optical flow constraint with a sub-grid transport equation by introducing an eddy-diffusivity model. The diffusion coefficient of the transport equation is selected empirically. Instead, a structural sub-grid model with an eddy viscosity for computing the small-scale diffusion factor is applied in [6]. These works show good estimation results. However, let us outline that these approaches still highly depend on a regularization parameter whose value is difficult to fix and which has no direct physical interpretation. Furthermore, an additional parameter associated with the turbulence model, which is also difficult to fix in practice, is introduced in the data term.

In this paper, we aim at proposing a novel formulation for turbulent fluid motion estimation with a different strategy. The main ideas and contributions of this work consist in reformulating the optical flow estimation problem through the introduction of turbulence modeling expressed under a location uncertainty principle. As derived in [17], the Eulerian velocity of a flow is decomposed into a large-scale component and a small-scale turbulent component. The latter one, specified as a random field and referred to as location uncertainty, gives rise to a modified transport equation [20] obtained from a stochastic expression of the Reynolds transport theorem [8], [17]. The resulting stochastic optical flow constraint equation includes the effects of the unresolved (so called sub-grid) velocity component. Another constraint on the kinetic energy enables us to interpret the regularizer as a physical constraint. As we demonstrate it in this paper, all the parameters involved in this optical flow model can be optimally set or estimated. Therefore, it enables us to avoid the inescapable and cumbersome parameter tuning.

## 2 Methodology Description

### 2.1 Stochastic transport

Let $\mathbf{x}_t = (x(t), y(t))^T$ ($\mathbf{x}_t \in \mathbb{R}^2$) denote the position of a particle in the two-dimensional (2D) domain $\Omega$ at time step $t$. Let us follow the basic assumption that the Eulerian velocity field of turbulent flow consists of a smooth velocity component $\omega(\mathbf{x},t) = (u,v)^T$ and a small-scale random velocity component termed uncertainty. Accordingly, the Lagrangian stochastic displacement regarding the trajectory $\mathbf{x}_t$ reads:

$$\mathrm{d}\mathbf{x}_t = \omega(\mathbf{x}_t,t)\mathrm{d}t + \sigma(\mathbf{x}_t,t)\mathrm{d}\mathbf{B}_t. \tag{2}$$

The integral expression involves a random function, $\mathbf{B}_t$, that can be interpreted as a white noise process in space and a Brownian process in time. The spatial correlations of the velocity uncertainty are specified through a diffusion operator $\sigma(\mathbf{x},t)$ defined through the matrix kernel $\breve{\sigma}(\cdot,\cdot,t)$ for any vectorial function $\boldsymbol{f}$ (n-dimensional) as:

$$\sigma(\mathbf{x},t)\boldsymbol{f} \triangleq \int_\Omega \breve{\sigma}(\mathbf{x},\mathbf{z},t)\boldsymbol{f}(\mathbf{z},t)\mathrm{d}\mathbf{z}. \tag{3}$$

Therefore, it can be seen that this operator is a matrix mapping from $\mathbb{R}^n$ into $\mathbb{R}^2$ at point $\mathbf{x}$. In a motion estimation context, the flow velocity field is assumed constant between two successive image frames. Then without loss of generality we can safely ignore the time variable of $\omega(\mathbf{x},t)$ and $\sigma(\mathbf{x},t)$. Thus we have $\mathrm{d}\mathbf{x} = \omega(\mathbf{x})\mathrm{d}t + \sigma(\mathbf{x})\mathrm{d}\mathbf{B}_t$, where $\mathrm{d}\mathbf{x} = \mathbf{x}_t - \mathbf{x}_{t-1}$ represents the displacements of particles between two successive images. The uncertainty component, $\sigma(\mathbf{x})\mathrm{d}\mathbf{B}_t$, representing the small-scale velocity, is a Gaussian random function correlated in space. The covariance tensor of the uncertainty component $\sigma\mathrm{d}\mathbf{B}_t$ (at different locations - $\mathbf{x}$ and $\mathbf{x}'$) reads:

$$\begin{aligned} Q &= Cov(\mathbf{x},\mathbf{x}') \\ &\triangleq \mathbb{E}\left[(\sigma(\mathbf{x})\mathrm{d}\mathbf{B}_t)(\sigma(\mathbf{x}')\mathrm{d}\mathbf{B}_t)^T\right] = \int_\Omega \breve{\sigma}(\mathbf{x},\mathbf{z})\breve{\sigma}^T(\mathbf{x}',\mathbf{z})\mathrm{d}\mathbf{z}\,\mathrm{d}t = \sigma(\mathbf{x})\sigma^T(\mathbf{x}')\,\mathrm{d}t, \end{aligned} \tag{4}$$

where $\mathbb{E}\left[(\mathrm{d}\mathbf{B}_t)(\mathrm{d}\mathbf{B}_t)^T\right] = \mathrm{d}t$. The corresponding variance tensor, $\boldsymbol{a}$, is defined by the single-point covariance of the small-scale displacement. It is a $2\times 2$ symmetric positive definite matrix for each spatial point $\mathbf{x}$ in the 2D physical domain $\Omega$, given by:

$$\boldsymbol{a}(\mathbf{x}) \triangleq \sigma(\mathbf{x})\sigma^T(\mathbf{x}) = \int_\Omega \breve{\sigma}(\mathbf{x},\mathbf{z})\breve{\sigma}^T(\mathbf{x},\mathbf{z})\mathrm{d}\mathbf{z} = \frac{Cov(\mathbf{x},\mathbf{x})}{\mathrm{d}t}. \tag{5}$$

Given the stochastic formalism, we now consider that a conserved scalar quantity $f$ is transported by a motion field under location uncertainty. The conservation law reads:

$$f(\mathbf{x}_t + \mathrm{d}\mathbf{x}_t, t+\mathrm{d}t) = f(\mathbf{x}_t,t). \tag{6}$$

As $f$ is a random function, its material derivative $D_t f \triangleq \mathrm{d}f(\mathbf{x},t) = 0$, which involves the composition of two stochastic processes, can be expanded via the generalized Ito formula (Ito-Wentzell formula). The expression is given by

$$D_t f = \mathrm{d}_t f + \nabla f \cdot (\omega\mathrm{d}t + \sigma\mathrm{d}\mathbf{B}_t) + \sum_{i=1}^{2} \mathrm{d}\langle \frac{\partial f}{\partial \mathbf{x}_i}, \mathbf{x}_i\rangle \mathrm{d}t + \frac{1}{2}\sum_{i,j=1}^{2} \boldsymbol{a}_{ij}\frac{\partial^2 f}{\partial \mathbf{x}_i \partial \mathbf{x}_j}\mathrm{d}t, \tag{7}$$

where $\mathrm{d}_t f$ stands for the time increment of the (non differentiable) quantity $f$: $\mathrm{d}_t f = f(x,t+\mathrm{d}t) - f(x,t)$ and the quadratic variation operator $\langle \cdot, \cdot \rangle$ is briefly presented in the Appendix A. Compared to the standard Ito formula, the expression introduces the additional co-variation terms between $\mathbf{x}$ and the gradient of the random function $f$. The derivation of (7) is provided in details in [17] and [20], here we give the conclusion: for an incompressible random velocity component (namely $\nabla \cdot \sigma \mathrm{d}\mathbf{B}_t = 0$), the material derivative $D_t f$ has a simple form $\mathbb{D}_t$ as following

$$\mathbb{D}_t f = \mathrm{d}_t f + \left[ \nabla f \cdot \omega^* - \frac{1}{2} \nabla \cdot (\boldsymbol{a} \nabla f) \right] \mathrm{d}t + \nabla f \cdot \sigma \mathrm{d}\mathbf{B}_t, \tag{8}$$

which is refered to as the stochastic transport operator, where $\omega^*$ is the modified large-scale velocity that takes into account the inhomogeneity of the small-scale random velocity component:

$$\omega^* = \omega - \frac{1}{2} (\nabla \cdot \boldsymbol{a})^T. \tag{9}$$

This velocity corresponds to a correction of the large-scale velocity induced by the small scales inhomogeneity. The induced statistical velocity $(\nabla \cdot \boldsymbol{a})$ is a drift going from the variance tensor maxima to the variance tensor minima.

Compared to the deterministic material derivative, several additional terms related to the uncertainty random field are now involved in the formulation (8). A transport by the small-scale component is visible in the last right-hand side term of (8). The uncertainty term has also a mixing effect on the large-scale motion through a diffusion term along the proper directions of the variance tensor (third term of the right-hand side of (8)). Note that there are possibly a lot of degrees of freedom to define the diffusion tensor $\boldsymbol{a}$. In this study, in order to demonstrate the potential of this formalization we will only consider a simple isotropic divergence free model. This condition leads to a constant uncertainty for the whole domain between two successive samples, i.e., $\boldsymbol{a}(\mathbf{x}) = \alpha \mathbb{I}_2 = \text{const.}$, where $\mathbb{I}_2$ is the $2 \times 2$ identity matrix, hence $\nabla \cdot \boldsymbol{a}(\mathbf{x}) = 0$ and then $\omega^* = \omega$ due to (9). Therefore, in this case the stochastic transport equation (8) can be simplified as follow:

$$\mathbb{D}_t f = \mathrm{d}_t f + \left( \nabla f \cdot \omega - \frac{1}{2} \alpha \Delta f \right) \mathrm{d}t + \nabla f \cdot \sigma \mathrm{d}\mathbf{B}_t, \tag{10}$$

where $\Delta$ is the Laplacian operator. In the next section this expression of the material derivative enables us to derive an optical flow formulation under location uncertainty.

### 2.2 Data term based on stochastic model

From the previous stochastic transport equation, a novel observation term for optical flow estimation can be proposed. Hereafter, the conserved quantity $f$ is assumed to be proportional to the image intensity. Since the Brownian random terms have zero mean, one can take the expectation of (10) to derive the mean scalar advection, namely

$$\mathbb{E}(\mathbb{D}_t f) = \mathbb{E}\left[ \mathrm{d}_t f + \left( \nabla f \cdot \omega - \frac{1}{2} \alpha \Delta f \right) \mathrm{d}t \right]. \tag{11}$$

The data term of the motion estimation cost functional can be set as the variance of the luminance variation:

$$\begin{aligned} e_{data} =& \mathbb{E}[(\mathbb{D}_t f - \mathbb{E}(\mathbb{D}_t f))^2] \\ \approx& \int_\Omega \left[ \mathrm{d}_t f + \left( \nabla f \cdot \boldsymbol{\omega} - \frac{1}{2}\alpha \Delta f \right) \mathrm{d}t \right]^2 \mathrm{d}\mathbf{x} - \int_\Omega \left( \beta^2 \alpha |\nabla f|^2 \mathrm{d}t \right) \mathrm{d}\mathbf{x}. \end{aligned} \tag{12}$$

where $|\cdot|$ denotes the Euclidean norm, i.e., $|\nabla f|^2 = (\partial_x f)^2 + (\partial_y f)^2$. The derivation in (12) is thoroughly given in Appendix A. In this expression an additional coefficient $\beta$ has to be fixed or estimated. An estimate of this parameter is also provided in Appendix A. As all the quantities involved are assumed to be constant in time between two consecutive images, $\mathrm{d}t$ can be replaced by the time interval between the two frames and adimensioned to 1. Note that if the investigated flow is fully resolved or contains no location uncertainty (i.e., the variance factor of the uncertainty component $\boldsymbol{a} = \alpha \mathbb{I}_2 = \mathbf{0}$), the simplified version of (12) boils down exactly to the classical optical flow constraint equation. The data model is the sum of two quadratic terms. The first one has the form of a modified OFC equation. This new brightness consistancy model includes a diffusion of the image brightness, which represents the unresolved scales action on the transported luminance function. As for the second term, it can be observed that it corresponds to a weighting of the luminance energy dissipation. It can be thus seen as the measure of the mean transported scalar energy evolution on the time interval between two consecutive images.

### 2.3 Regularization term dedicated to stochastic transport

Generally, the regularization term in motion estimation cost functionals is set from a regularity condition on the solution. Such assumption is difficult to relate to kinematical or dynamical properties of the flow. In this section, we explain the spatial regularizer ensuing from an energy conservation assumption. Based on the stochastic transport presented in Section 2.1, a stochastic representation of the Navier-Stokes equations has been derived in [17]. By neglecting the external and conservative forces, the dynamics of the stochastic flow (namely momentum equation under location uncertainty) has the following expression:

$$\frac{\partial \omega_i}{\partial t} + (\boldsymbol{\omega} \cdot \nabla)\, \omega_i - \frac{1}{2}\alpha \Delta\, \omega_i = 0, \tag{13}$$

where $\boldsymbol{\omega}$ and $\boldsymbol{a} = \alpha \mathbb{I}_2$ are defined in the same way as (10), and $i$ stands for the component of $x$-direction or $y$-direction, i.e., $\omega_i = u$ or $v$. An inner product with the velocity of equation (13) followed by integrations by parts provides the kinetic energy evolution:

$$\frac{\partial}{\partial t} E_{kin} = \frac{1}{2}\frac{\partial}{\partial t} \| \boldsymbol{\omega} \|_2^2 = -\frac{1}{2} \int_\Omega \sum_i \alpha |\nabla \omega_i|^2 \mathrm{d}\mathbf{x}. \tag{14}$$

In order to obtain a transformation from one image to the subsequent one that tends to conserve the kinetic energy, we can expect the semi-norm appearing in the right-hand-side of (14) to be as small as possible, i.e.,

$$e_{reg} = \frac{1}{2} \int_\Omega \alpha \| \nabla \boldsymbol{\omega} \|_F^2 \, \mathrm{d}\mathbf{x} = \frac{1}{2} \int_\Omega \alpha \left( |\nabla u|^2 + |\nabla v|^2 \right) \mathrm{d}\mathbf{x}, \tag{15}$$

where $\|\cdot\|_F$ denotes the Frobenius norm for a matrix. We remark that the regularizer (15) is the same as the usual gradient penalizer except for the introduction of the diffusion factor $\alpha$. Therefore, the classical gradient smoothing penalization can be interpreted as derived from a homogeneous divergence-free uncertainty random field [17]. This basic model yields a smoothing term with no preferential direction.

*Remark 1.* It is necessary to discuss here the unit of the covariance factor $\boldsymbol{a} = \alpha\mathbb{I}_2$. According to the principle that different terms in a physical equation should have the same unit, we now examine the units of the different terms in the momentum transport equation (13). By letting $\lceil g \rfloor$ denote the unit of function $g$, we have: $\lceil \frac{\partial \omega}{\partial t} \rfloor = \mathrm{L}/\mathrm{T}^2$, where L and T denote the basic units of length and time, respectively. That means the unit of the third term in (13) should satisfy:

$$\lceil \alpha \Delta \omega \rfloor = \lceil \alpha \rfloor \cdot \lceil \Delta \omega \rfloor = \lceil \alpha \rfloor \cdot \frac{1}{\mathrm{TL}} = \frac{\mathrm{L}}{\mathrm{T}^2}.$$

Hence, we obtain the units of $\alpha$, the data term and the regularization term as follows:

$$\lceil \alpha \rfloor = \frac{\mathrm{L}^2}{\mathrm{T}}, \quad \lceil e_{data} \rfloor = \frac{\mathrm{I}^2}{\mathrm{T}^2}, \quad \lceil e_{reg} \rfloor = \frac{\mathrm{L}^2}{\mathrm{T}^3}, \tag{16}$$

where I denotes the basic unit of the luminance function (greyscale unit), and in practice, the unit of time is adimensioned with the time difference between two samples and therefore set to 1. To balance the two terms, a weighting coefficient with unit $\mathrm{I}^2/\mathrm{L}^2$ must be introduced.

Gathering the data term and the regularization term, the final energy functional reads:

$$J = \int_\Omega \left[ \left( \mathrm{d}_t f + \nabla f \cdot \omega - \frac{1}{2}\alpha \Delta f \right)^2 - \beta^2 \alpha |\nabla f|^2 \right] \mathrm{d}\mathbf{x} + \int_\Omega \frac{1}{2}\lambda \alpha \parallel \nabla \omega \parallel_F^2 \mathrm{d}\mathbf{x}, \tag{17}$$

where $\lambda$ is a positive weight coefficient. In traditional optical flow methods the weighting coefficient balancing the data term and the regularizer is a very sensible parameter that is difficult to tune since $\lambda$ is not directly related to any physical quantity such as the motion amplitude. In this paper, by dimensional analysis of the objective functional (discussed in Remark 1), we find that $\lambda$ should have the unit of $\mathrm{I}^2/\mathrm{L}^2$. That means $\lambda$ can be related to the gradient of image intensity. Therefore, from this point of view, there are several choices can be used to formulate $\lambda$:

$$\lambda_1 = \frac{1}{\Omega}\int_\Omega \frac{(\mathrm{d}_t f)^2}{(L_{\max})^2}\mathrm{d}\mathbf{x}, \quad \lambda_2 = \frac{1}{\Omega}\int_\Omega \left(\mathrm{d}_t \mid \nabla f \mid^2\right)\mathrm{d}\mathbf{x}, \quad \lambda_3 = \frac{1}{\Omega}\int_\Omega \left(\mid \mathrm{d}_t \nabla f \mid^2\right)\mathrm{d}\mathbf{x}, \tag{18}$$

where $L_{\max}$ represents a characteristic value of the length scale in the images, which can be given by the maximum magnitude of the apparent displacements. We will evaluate these candidates in the experimental section.

The resulting energy functional (17) resembles to a simple modification of the Horn & Schunk functional. However, in this new formulation, the penalization constant of the smoothing term is now interpreted as the variance of the small-scale unresolved motion. This variance parameter $\alpha$ now also appears as the weighting factor of two additional terms in the data adequacy terms. As explained in the next section, this property will allow us to optimally estimate the variance parameter.

## 3 Minimization and Implementation

In this section we detail the computation of the cost functional optimum with respect to the two unknowns: $\omega$ and $\alpha$. The optimization algorithm is performed through an alternated minimization of the two variables.

### 3.1 Minimization with respect to the motion field

Let us assume that an initial $\alpha$ is known (in our paper, alpha is initialized with a fixed value 0.5 for both synthetic and real-world image sequences), $\mathrm{d}_t f \triangleq f_t$, $\nabla f = (\partial_x f, \partial_y f) \triangleq (f_x, f_y)$. By applying the calculus of variation (Euler-Lagrange equation) to (17), we have

$$\begin{cases} 2\left(f_x u + f_y v + f_t - \dfrac{1}{2}\alpha\Delta f\right) f_x - 2\cdot\dfrac{1}{2}\lambda\alpha\Delta u = 0, \\ 2\left(f_x u + f_y v + f_t - \dfrac{1}{2}\alpha\Delta f\right) f_y - 2\cdot\dfrac{1}{2}\lambda\alpha\Delta v = 0. \end{cases} \tag{19}$$

With the approximations of Laplacians $\Delta u \approx \kappa(\bar{u}-u)$, $\Delta v \approx \kappa(\bar{v}-v)$, where $\bar{u}$, $\bar{v}$ denote the local averages and $\kappa$ depends on the difference scheme, (19) can be expressed as the following equations:

$$\begin{cases} \left(f_x^2 + \dfrac{1}{2}\lambda\alpha\right) u + f_x f_y v = \dfrac{1}{2}\lambda\alpha\bar{u} + \dfrac{1}{2}\alpha f_x\Delta f - f_x f_t, \\ f_x f_y u + \left(f_y^2 + \dfrac{1}{2}\lambda\alpha\right) v = \dfrac{1}{2}\lambda\alpha\bar{v} + \dfrac{1}{2}\alpha f_y\Delta f - f_y f_t, \end{cases} \tag{20}$$

which can be solved by the Gauss-Seidel method or the Successive Over Relation (SOR) iteration. In our algorithm, by applying elimination method to (20), the velocity vector $\omega$ can be computed by the following iterative formulation:

$$\begin{cases} u^{k+1} = \bar{u}^k - \dfrac{f_x\bar{u}^k + f_y\bar{v}^k + f_t - \frac{1}{2}\alpha\Delta f}{\frac{1}{2}\lambda\alpha + f_x^2 + f_y^2} f_x, \\ v^{k+1} = \bar{v}^k - \dfrac{f_x\bar{u}^k + f_y\bar{v}^k + f_t - \frac{1}{2}\alpha\Delta f}{\frac{1}{2}\lambda\alpha + f_x^2 + f_y^2} f_y. \end{cases} \tag{21}$$

### 3.2 Estimation of diffusion factor

The most important parameter to estimate the large-scale velocity field, $\omega$, is the diffusion factor $\alpha$. Since $\alpha$ can be regarded as an unknown in the objective functional (17), one can compute $\alpha$ by cancelling the energy functional gradient with respect to this variable. Therefore, we have

$$\begin{aligned} \frac{\partial J}{\partial \alpha} = &\int_\Omega \left[\Delta f\left(\partial_t f + \nabla f\cdot\omega - \frac{1}{2}\alpha\Delta f\right) - \beta^2|\nabla f|^2\right] \mathrm{d}\mathbf{x} \\ &+ \int_\Omega \frac{1}{2}\lambda \parallel \nabla\omega \parallel_F^2 \mathrm{d}\mathbf{x} = 0. \end{aligned} \tag{22}$$

Then we readily obtain

$$\hat{\alpha}^{k+1} = 2\frac{\int_\Omega \left[\Delta f\left(\nabla f \cdot \bar{\omega}^k + f_t\right) + \beta^2 \mid \nabla f \mid^2 - \frac{1}{2}\lambda \parallel \nabla \bar{\omega}^k \parallel_F^2\right] \mathrm{d}\mathbf{x}}{\int_\Omega (\Delta f)^2 \mathrm{d}\mathbf{x}}, \tag{23}$$

where $\bar{\omega}^k$ is the estimated velocity vector from the previous iteration, defined by (21).

### 3.3 Multi-resolution algorithm

For the basic optical flow methods, one common weakness is that the procedure can yield good results only when the magnitude of image motions is small (smaller than the shortest spatial wavelength present in the image [12]). To overcome the estimation issue due to the large displacements, we use an incremental coarse-to-fine strategy. The main idea of this strategy can be divided into several processes: a) a multi-resolution representation through the successive Gaussian filtering and sub-sampling is applied to the images pair; b) the optical flow is computed from the coarse-resolution level and then projected onto the next finer level of the pyramid; in the projection step, image warping is required so we only need to compute the small velocity increments at the higher resolution level; c) this process is repeated at finer and finer spatial scales until the original image resolution is reached. The choice of the image filtering process is significant for the multi-resolution algorithm. Gaussian filters are applied to the original images to reduce the noise effect. Furthermore, median filters are applied to the estimated velocity fields after each warping step for the purpose of eliminating the outliers. For more details of the coarse-to-fine algorithm we refer to [21]. The framework of the multi-resolution strategy is shown in Algorithm 1.

## 4 Experimental Results

### 4.1 Synthetic Image sequence

A synthetic fluid image sequence[3] is tested in this section, which is provided by [4] and generated by Direct Numerical Simulation (DNS). The phenomenon investigated is the spreading of a low diffusivity dye in a 2D homogeneous turbulent flow with Reynolds number $Re = 3000$ and Schmidt number $Sc = 0.7$. The intensity of the passive scalar images is proportional to the dye concentration. The sequence consists of 100 successive images at the resolution of $256 \times 256$ pixels. An example of the scalar image and the corresponding vorticity map are displayed in Figure 1 (a) and (b). A multi-resolution algorithm with 2 levels and 5 warping steps at each level has been implemented. As for the computation of $\lambda$, we use the first formulation in (18) by default.

To evaluate quantitatively the estimated motion fields, we follow a standard way by computing the average angular error (AAE) and root mean square error (RMSE) over $N$ pixels of the image:

$$AAE = \frac{1}{N}\sum_{i=1}^{N} \arccos \frac{u_i^t u_i^e + v_i^t v_i^e + 1}{\sqrt{(u_i^t)^2 + (v_i^t)^2 + 1}\sqrt{(u_i^e)^2 + (v_i^e)^2 + 1}}, \tag{24}$$

$$RMSE = \sqrt{\frac{1}{N}\sum_{i=1}^{N} [(u_i^t - u_i^e)^2 + (v_i^t - v_i^e)^2]}, \tag{25}$$

[3] Available online: `http://fluid.irisa.fr/`

**Algorithm 1:** Multi-resolution algorithm with symmetric warping for motion estimation

**Load image pair** $Img_1$ **and** $Img_2$;
Pre-processing;
**Pyramidal generation** from level 0 (original) to L (coarsest);
Compute the weighting coefficient $\lambda$ ;
**for** $l = L$ *to* 0 **do**
  **if** $l = L$ **then**
    Set initial velocities be 0 at coarsest level $\widehat{\omega_{l+1}} = 0$;
    Set initial estimation of $\alpha$;
  **else**
    Expand the velocities from coarser level $\omega_{l+1}$ to finer level $\widehat{\omega_{l+1}}$ by interpolation;
    Set $\alpha$ the estimated $\alpha$ from the previous level;
  **end**
  **for** *Each warping step* **do**
    **Symmetric warping**
      $f_1 = warpForward(Img_1^l)$, $f_2 = warpInverse(Img_2^l)$.
    **Optimization**
      Compute the gradients and Laplacians $f_t$, $\nabla f$, $\Delta f$;
      Compute the estimation of $\beta^2$;
      Estimate the motion field $\mathrm{d}\omega$ and $\alpha$ by iterations (21) and (23), respectively;
      Update $\omega_l = \widehat{\omega_{l+1}} + \mathrm{d}\omega$;
    **Median filtering**
  **end**
**end**
**End** multi-resolution;

where $(u^t, v^t)$ and $(u^e, v^e)$ denote the ground-truth velocity and the estimated velocity, respectively. The index $i$ represents the pixel where optical flow is computed. Furthermore, vorticity maps which are computed by $(\partial_x v - \partial_y u)$ are also demonstrated.

The estimated motion field and vorticity map at time step $t = 50$ are illustrated in Figure 1, in comparison with the methods of [13], [10], and [11]. We can observe from the vorticity maps that the proposed stochastic formulation performs better than the other references, especially in the area with high vorticity. The vortex structures are well recovered by the proposed optical flow formulation, whereas they are blurred by the HS method. The methods of [10] and [11] achieve to estimate the large-scale structures of the flow. However, they fail to provide the small-scale components in some areas. Figure 2 illustrates the result of a typical area of the scalar image with a strong vortex. A zoom in this region shows that the estimated velocity field (black vectors) is highly consistent with the ground-truth (red vectors).

Quantitative evaluations for the DNS passive scalar images are given in Figure 3. The AAE and RMSE errors of the proposed method and the HS method are plotted in

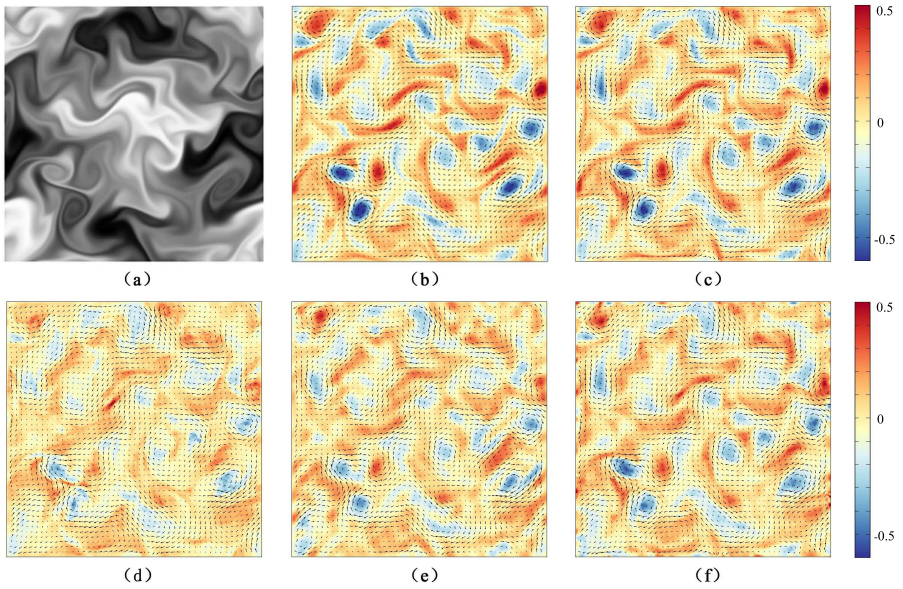


**Fig. 1.** Velocity fields and vorticity maps estimated from different methods on DNS passive scalar image sequence at $t = 50$: (a) scalar image; (b) ground-truth; (c) proposed method; (d) HS method; (e) method of [10]; (f) method of [11].

Figure 3 (a) and (b), respectively. It can be seen that the accuracy is drastically improved by more than 50% for both the AAE and the RMSE. Even compared with the state-of-the-art approaches, the proposed method shows the best performances. Error data of the other optical flow methods, including [22], [10], [11], [15], and [6], are taken from [6] and displayed in Figure 3 (c) and (d). The results of our method is close to (slightly better than) the results of [6], which applies a data term based on the large eddy simulation (LES) sub-grid model and a divergence-free regularization term. Both the proposed technique and [6] outperform the other methods for the whole passive scalar image sequence, indicating that the introduction of turbulence models is significant for fluid motion estimation. The method of [6] depends on several parameters: the standard deviation of a low-pass filtering applied on the sequence, the regularization coefficient, and the ratio of the Reynolds and Schmidt numbers of the flow. These constants are difficult to fix or not available with accuracy in practice, and must be adapted from one sequence to the other. On the contrary, the estimator under uncertainty proposed in this paper does not require such a tuning and can be qualified as a parameter-free approach.

Finally, Figure 4 shows the impact of different choices for lambda, which have the same required unit. As we can see, although those candidates give different values of $\lambda$, they provide similar estimation results of the velocity field. We conclude that one can choose any of them to construct a parameter-free estimator.

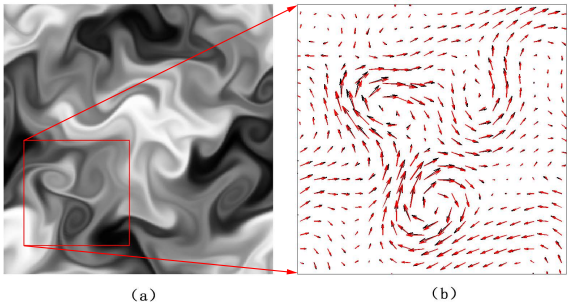


**Fig. 2.** Velocity vectors on DNS passive scalar image sequence at $t = 50$: (a) scalar image with zoomed area; (b) true velocity vectors (red) and the estimated vectors by the proposed method (black).

### 4.2 Real Images

An experimental image sequence of 2D turbulence is provided by [14]. The authors presented the first detailed experimental observation of the Batchelor regime [1], in which a passive scalar was dispersed by a large-scale strain. Two successive frames of this sequence are displayed in Figure 5 (a) and (b), respectively. The strong turbulent vortices can be clearly observed. We implement a multi-resolution algorithm with 5 levels and 2 warping steps at each multi-resolution level . Figure 5 (c), (d) demonstrate the vorticity maps estimated from the HS method and the proposed method. It can be seen that the result of the HS method is over-smoothed, while the result of the proposed formulation shows more finer structures on the vorticity map.

## 5 Conclusion

In this paper, we introduce a variational optical flow formulation for turbulent fluid motion estimation. This novel formulation is derived from a location uncertainty principle [17], which enables us to take into account the small-scale unresolved components of the velocity field, and also allows us to estimate explicitly the different parameters involved. The experimental results on both synthetic and real image sequences indicate the efficiency of the proposed parameter-free technique.

## A Variance of Stochastic Transport Operator

Before deriving the variance of the stochastic transport operator, we first recall briefly the notions of quadratic variation and covariation, which are important in stochastic calculus. Suppose that $X_t$, $Y_t$ are stochastic processes defined on the probability space $(\Omega, \mathscr{F}, \mathbb{P})$, the quadratic covariation process denoted as $\langle X, Y \rangle_t$, is defined as the limit in probability:

$$\langle X, Y \rangle_t = \lim_{\delta t_i \to 0} \sum_{i=0}^{n-1} \left( X_{t_{i+1}} - X_{t_i} \right) \left( Y_{t_{i+1}} - Y_{t_i} \right)^T, \tag{26}$$

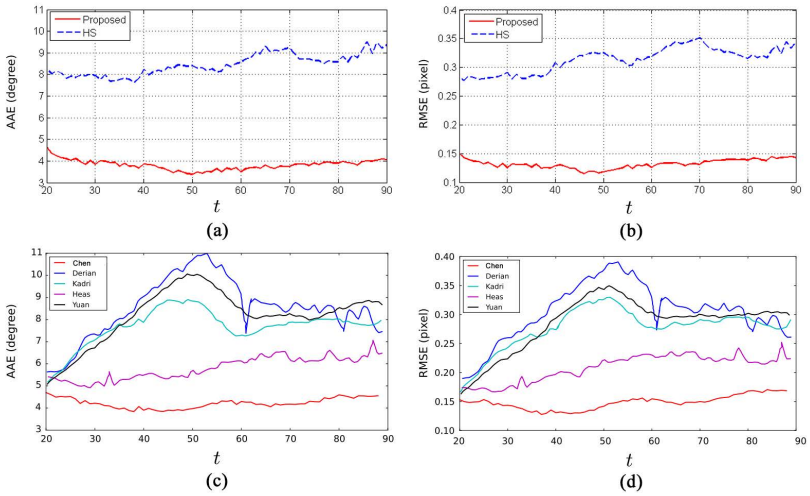


**Fig. 3.** AAE (left) and RMSE (right) errors of different estimators for DNS scalar image sequence. Results of the proposed method are plotted in figures (a) and (b), in comparison with the results of the HS method. Results of several state-of-the-art approaches are shown in figures (c) and (d).

with $t_1 < t_2 < \cdots < t_n$ and $\delta t_i = t_{i+1} - t_i$. For the Brownian motion, the quadratic covariances can be computed by the following rules:

$$\langle B, B\rangle_t = t, \quad \langle B, h\rangle_t = \langle h, B\rangle_t = \langle h, h\rangle_t = 0, \tag{27}$$

where $h$ is a deterministic function and $B$ denotes a Brownian process. Now we can recall the stochastic transport of a scalar $f$ and its expectation, i.e., equations (10) and (11). Assuming a stationary distribution, then the expectation is the solution of a stationary equation and $\mathbb{E}(\mathbb{D}_t f) = 0$. Therefore, the variance of the stochastic transport operator is expressed as:

$$\begin{aligned} Var(\mathbb{D}_t f) =& \mathbb{E}\left[(\mathbb{D}_t f - \mathbb{E}(\mathbb{D}_t f))^2\right] = \mathbb{E}\left[(\mathbb{D}_t f)^2\right] \\ =& \mathbb{E}\left\{\left[\mathrm{d}_t f + \left(\nabla f \cdot \omega - \frac{1}{2}\alpha\Delta f\right)\mathrm{d}t\right]^2\right\} + \mathbb{E}\left\{(\nabla f \cdot \sigma \mathrm{d}\mathbf{B}_t)^2\right\} \\ &+ \mathbb{E}\left\{2\left[\mathrm{d}_t f + \left(\nabla f \cdot \omega - \frac{1}{2}\alpha\Delta f\right)\mathrm{d}t\right](\nabla f \cdot \sigma \mathrm{d}\mathbf{B}_t)\right\}, \end{aligned} \tag{28}$$

where the second term and the third term involve a Brownian term. According to the Itô isometry, we obtain:

$$\mathbb{E}\left\{(\nabla f \cdot \sigma \mathrm{d}\mathbf{B}_t)^2\right\} = \mathbb{E}\left\{\langle \nabla f \cdot \sigma \mathrm{d}\mathbf{B}_t,\ \nabla f \cdot \sigma \mathrm{d}\mathbf{B}_t\rangle\right\} = \mathbb{E}\left\{\left(\alpha |\nabla f|^2\right)\mathrm{d}t\right\} \tag{29}$$

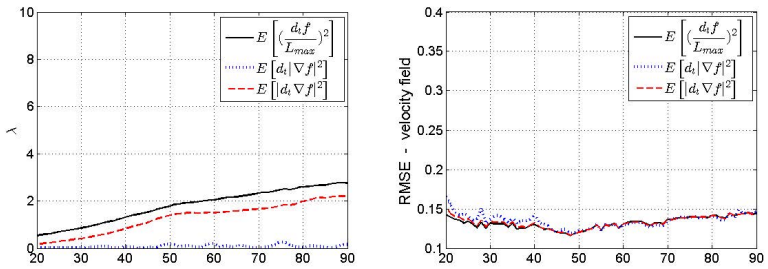


**Fig. 4.** The values of different choices for the weighting coefficient $\lambda$ (left) and the corresponding estimated RMSE results (right) on DNS scalar images. The notation $E$ denotes the mean value over the image domain.

and

$$\begin{aligned}&\mathbb{E}\left\{2\left[\mathrm{d}_t f+\left(\nabla f\cdot\omega-\frac{1}{2}\alpha\Delta f\right)\mathrm{d}t\right](\nabla f\cdot\sigma\mathrm{d}\mathbf{B}_t)\right\}\\ =&2\mathbb{E}\left\{\left\langle \mathrm{d}_t f+\left(\nabla f\cdot\omega-\frac{1}{2}\alpha\Delta f\right)\mathrm{d}t,\ \nabla f\cdot\sigma\mathrm{d}\mathbf{B}_t\right\rangle\right\}=2\mathbb{E}\left\{\langle \mathrm{d}_t f,\ \nabla f\cdot\sigma\mathrm{d}\mathbf{B}_t\rangle\right\},\end{aligned} \tag{30}$$

where (30) represents the correlation between the martingale part of $\mathrm{d}_t f$ and the random advection term $\nabla f\cdot\sigma\mathrm{d}\mathbf{B}_t$. For a conserved quantity $f$, we have the transport equation $\mathbb{D}_t f=0$. This implies that when separating $f=\tilde{f}+f'$ in terms of its bounded variation part and its martingale part (i.e., time scale separation in terms of $\mathrm{d}t$ and $\mathrm{d}\mathbf{B}_t$, which is a unique decomposition), the transport equation can be separated into:

$$\begin{cases}\dfrac{\partial\tilde{f}}{\partial t}\mathrm{d}_t+\left(\nabla f\cdot\omega-\dfrac{1}{2}\alpha\Delta f\right)\mathrm{d}t=0,\\ \qquad\qquad \mathrm{d}_t f'+\nabla f\cdot\sigma\mathrm{d}\mathbf{B}_t=0.\end{cases} \tag{31}$$

Thus, we have

$$\begin{aligned}0&=\left\langle \mathrm{d}_t f'+\nabla f\cdot\sigma\mathrm{d}\mathbf{B}_t,\ \mathrm{d}_t f'+\nabla f\cdot\sigma\mathrm{d}\mathbf{B}_t\right\rangle,\\ &=\left\langle \mathrm{d}_t f',\ \mathrm{d}_t f'\right\rangle+\left\langle\nabla f\cdot\sigma\mathrm{d}\mathbf{B}_t,\ \nabla f\cdot\sigma\mathrm{d}\mathbf{B}_t\right\rangle+2\left\langle \mathrm{d}_t f',\ \nabla f\cdot\sigma\mathrm{d}\mathbf{B}_t\right\rangle.\end{aligned} \tag{32}$$

Note that $\langle \mathrm{d}_t f',\ \mathrm{d}_t f'\rangle=\langle \mathrm{d}_t f,\ \mathrm{d}_t f\rangle$, since the quadratic variation of bounded variation functions (such as the deterministic functions) is equal to 0. Equation (31) shows that in the case of a transported quantity $\mathrm{d}_t f'=-\nabla f\cdot\sigma\mathrm{d}\mathbf{B}_t$. When the conservation does hold only approximately (as in the case of the brightness consistency assumption), we will assume the proportionality relation: $\mathrm{d}_t f'=\beta\nabla f\cdot\sigma\mathrm{d}\mathbf{B}_t$, where $\beta$ has to be fixed or estimated (note that $\beta=-1$ for a strict stochastic transport). This assumption comes to assume that the highly fluctuating part of the intensity difference is explained by the transport of the luminance function by the small-scale motion up to a proportionality factor. With this assumption we have:

$$\mathbb{E}\left\{\left\langle \mathrm{d}_t f',\ \mathrm{d}_t f'\right\rangle\right\}=\mathbb{E}\left\{\langle\beta\nabla f\cdot\sigma\mathrm{d}\mathbf{B}_t,\ \beta\nabla f\cdot\sigma\mathrm{d}\mathbf{B}_t\rangle\right\}=\beta^2\mathbb{E}\left\{\left(\alpha|\nabla f|^2\right)\mathrm{d}t\right\}. \tag{33}$$

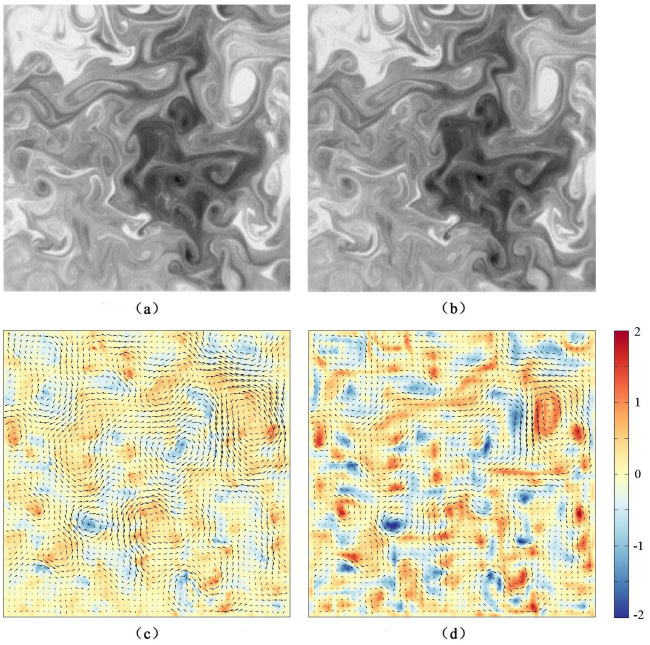


**Fig. 5.** Results on experimental scalar images: (a) first frame; (b) second frame; (c) estimated velocity field and vorticity map from the HS method; (d) estimated velocity field and vorticity map from the proposed method.

An estimate of $\beta$ from this equation can be readily obtained: $\beta^2 = \mathbb{E}\left[\frac{(\mathrm{d}_t f')^2}{\alpha|\nabla f|^2}\right]$.
In practice the fluctuation $f' = f - \tilde{f}$ is set as the difference between the luminance function and a local (spatial/temporal) mean $\bar{f}$. For successive images, the temporal difference is thus $\mathrm{d}_t f' = f_2' - f_1' = (f_2 - \bar{f}_2) - (f_1 - \bar{f}_1)$. Note that as $\boldsymbol{a}$ is also an unknown in the optical flow formulation. This leads to an interleaved optimization problem. Here we adopt a simpler strategy in which the proportionality coefficient is fixed from the value of $\boldsymbol{a}$ at the previous multi-resolution level (i.e., $\boldsymbol{a}^{L-1}$). Eventually, by combining (32), (33) and (29), it yields

$$2\mathbb{E}\left\{\left\langle \mathrm{d}_t f', \nabla f \cdot \sigma \mathrm{d}\mathbf{B}_t \right\rangle\right\} = -\mathbb{E}\left\{\left(\alpha|\nabla f|^2\right)\mathrm{d}t\right\} - \beta^2 \mathbb{E}\left\{\left(\alpha|\nabla f|^2\right)\mathrm{d}t\right\}. \tag{34}$$

Substituting these equations into (28), we finally obtain:

$$Var(\mathbb{D}_t f) \approx \mathbb{E}\left\{\left[\mathrm{d}_t f + \left(\nabla f \cdot \omega - \frac{1}{2}\alpha\Delta f\right)\mathrm{d}t\right]^2\right\} - \mathbb{E}\left\{\beta^2\alpha|\nabla f|^2\mathrm{d}t\right\}. \tag{35}$$

A minimum variance estimator with a spatial averaging for the expectation or considering a homogeneous Gaussian density leads to minimize:

$$Var(\mathbb{D}_t f) \approx \int_\Omega \left[\mathrm{d}_t f + \left(\nabla f \cdot \omega - \frac{1}{2}\alpha\Delta f\right)\mathrm{d}t\right]^2 \mathrm{d}\mathbf{x} - \int_\Omega \left(\beta^2\alpha|\nabla f|^2\mathrm{d}t\right)\mathrm{d}\mathbf{x}. \tag{36}$$

## References


1. G. Batchelor. Small-scale variation of convected quantities like temperature in turbulent fluid. *Journal of Fluid Mechanics*, 5(01):113–133, 1959.
2. M. Black and P. Anandan. The robust estimation of multiple motions: Parametric and piecewise-smooth flow fields. *Computer Vision and Image Understanding*, 63(1):75–104, 1996.
3. A. Bruhn, J. Weickert, and C. Schnörr. Lucas/Kanade meets Horn/Schunck: Combining local and global optic flow methods. *International Journal of Computer Vision*, 61(3):211–231, 2005.
4. J. Carlier. Second set of fluid mechanics image sequences. *European Project Fluid Image Analysis and Description (FLUID) - http://www.fluid.irisa.fr*, 2005.
5. C. Cassisa, S. Simoens, V. Prinet, and L. Shao. Subgrid scale formulation of optical flow for the study of turbulent flow. *Experiments in Fluids*, 51(6):1739–1754, 2011.
6. X. Chen, P. Zillé, L. Shao, and T. Corpetti. Optical flow for incompressible turbulence motion estimation. *Experiments in Fluids*, 56(1):1–14, 2015.
7. T. Corpetti, E. Mémin, and P. Pérez. Dense estimation of fluid flows. *IEEE Trans. on Pattern Analysis and Machine Intelligence*, 24(3):365–380, 2002.
8. D. Crisan, F. Flandoli, and D. Holm. Solution properties of a 3D stochastic Euler fluid equation. *arXiv preprint arXiv:1704.06989*, 2017.
9. A. Cuzol and E. Mémin. A stochastic filtering technique for fluid flow velocity fields tracking. *IEEE Tran. on Pattern Analysis and Machine Intelligence*, 31(7):1278–1293, 2009.
10. P. Dérian, P. Héas, C. Herzet, and E. Mémin. Wavelets and optical flow motion estimation. *Numerical Mathematics: Theory, Methods and Applications*, 6(1):116–137, 2013.
11. P. Héas, E. Mémin, D. Heitz, and P. Mininni. Power laws and inverse motion modeling: application to turbulence measurements from satellite images. *Tellus A: Dynamic Meteorology and Oceanography*, 64(10962), 2012.
12. D. Heitz, E. Mémin, and C. Schnörr. Variational fluid flow measurements from image sequences: synopsis and perspectives. *Experiments in Fluids*, 48(3):369–393, 2010.
13. B. Horn and B. Schunck. Determining optical flow. *Artificial Intelligence*, 17(1-3):185–203, 1981.
14. M. Jullien, P. Castiglione, and P. Tabeling. Experimental observation of Batchelor dispersion of passive tracers. *Physical Review Letters*, 85(17):3636, 2000.
15. S. Kadri-Harouna, P. Dérian, P. Héas, and E. Mémin. Divergence-free wavelets and high order regularization. *International Journal of Computer Vision*, 103(1):80–99, 2013.
16. T. Liu and L. Shen. Fluid flow and optical flow. *Journal of Fluid Mechanics*, 614:253–291, 2008.
17. E. Mémin. Fluid flow dynamics under location uncertainty. *Geophysical & Astrophysical Fluid Dynamics*, 108(2):119–146, 2014.
18. E. Mémin and P. Pérez. Dense estimation and object-based segmentation of the optical flow with robust techniques. *IEEE Trans. on Image Processing*, 7(5):703–719, 1998.
19. N. Papadakis and E. Mémin. Variational assimilation of fluid motion from image sequence. *SIAM Journal on Imaging Sciences*, 1(4):343–363, 2008.
20. V. Resseguier, E. Mémin, and B. Chapron. Geophysical flows under location uncertainty, Part I: Random transport and general models. *Geophysical & Astrophysical Fluid Dynamics*, 2017.
21. D. Sun, S. Roth, and M. Black. Secrets of optical flow estimation and their principles. In *Proc. of the IEEE Conf. on CVPR*, pages 2432–2439. IEEE, 2010.
22. J. Yuan, C. Schnörr, and E. Mémin. Discrete orthogonal decomposition and variational fluid flow estimation. *Journal of Mathematical Imaging and Vision*, 28(1):67–80, 2007.